

Kinetic Monte Carlo investigation of tetragonal strain on Onsager matricesZebo Li^{1,*} and Dallas R. Trinkle^{2,†}¹*Department of Nuclear, Plasma, and Radiological Engineering, University of Illinois, Urbana, Illinois 61801, USA*²*Department of Materials Science and Engineering, University of Illinois at Urbana-Champaign, Urbana, Illinois 61801, USA*

(Received 21 January 2016; published 17 May 2016)

We use three different methods to compute the derivatives of Onsager matrices with respect to strain for vacancy-mediated multicomponent diffusion from kinetic Monte Carlo simulations. We consider a finite difference method, a correlated finite difference method to reduce the relative statistical errors, and a perturbation theory approach to compute the derivatives. We investigate the statistical error behavior of the three methods for uncorrelated single vacancy diffusion in fcc Ni and for correlated vacancy-mediated diffusion of Si in Ni. While perturbation theory performs best for uncorrelated systems, the correlated finite difference method performs best for the vacancy-mediated Si diffusion in Ni, where longer trajectories are required.

DOI: [10.1103/PhysRevE.93.053305](https://doi.org/10.1103/PhysRevE.93.053305)**I. INTRODUCTION**

Stress or strain fields in crystalline solids play a crucial role in controlling the evolution and migration behavior of defects, leading to changes in material properties. External stress delays the coarsening kinetics of precipitates in superalloys [1] and influences the mobility of dislocations and grain boundaries [2–5]. Dislocations and grain boundaries, acting as sinks or sources of point defects, generate internal strain fields in their neighborhood, which affects the transport and segregation of vacancies, self-interstitials, and solute atoms [6–8]. In turn, changes in the transport properties of vacancies and interstitials also modify the climb rate of dislocations, and hence creep [9,10]. Moreover, the presence of stress or strain changes the formation energies of intrinsic point defects [11], which affects the migration behavior of solutes [12,13]. To predict mass transport in strained environments, the influence of strain on point defect and solute diffusion properties must be investigated.

Strain affects diffusion from a thermodynamic point of view by creating or modifying driving forces, and from a kinetic point of view by changing the transport coefficients or Onsager matrices [14], which connect the fluxes of species with the corresponding driving forces. Previous studies have mainly focused on strain effects on driving forces [15–18], but the strain-induced modification of Onsager matrices can also significantly change the diffusion behaviors. Dederichs *et al.* [19] have shown that the strain-induced anisotropy of saddle point configuration leads to an anisotropic diffusion even in materials which have cubic symmetry under zero stress. Garnier *et al.* [20] found that the strain field near an edge dislocation in Ni causes complex flow patterns for Si solutes and vacancies. Chan *et al.* [21] performed atomic simulations in face-centered cubic (fcc) Pt and Cu to show that the anisotropic diffusion of vacancies and self-interstitials under strain strongly depends on the crystal structure and the crystallographic directions in which the strain is applied. Sivak *et al.* [8] investigated the diffusion of point defects near edge dislocations in body-centered cubic (bcc) Fe and FCC Cu, and found that the dislocation strain fields induce

anisotropic migration of point defects. In all of these studies, the anisotropic diffusion behavior can be addressed from the strain dependence of Onsager matrices; however, only Garnier has calculated this effect using an analytical self-consistent mean field (SCMF) method [20].

Transport coefficients can be computed by combining two methods: kinetic Monte Carlo (KMC) [22] simulations and atomic-scale calculation of energy landscapes. KMC simulations use atomic jump rates to calculate the Onsager matrices for general systems. If the atomic jump rates follow the Arrhenius relationship, then the rate is determined by two quantities from the energy landscape: the attempt frequency and the migration energy. Migration energies, as well as their strain dependence, can be obtained from density functional theory (DFT) calculations [23]. Because KMC is a stochastic approach, the statistical errors make the strain derivatives of Onsager matrices more difficult to obtain than Onsager matrices themselves.

We derive three KMC-based methods to compute the derivatives of Onsager matrices with respect to strain for vacancy-mediated solute diffusion in fcc Ni. Migration energies for atomic jumps and their derivatives with respect to strains computed by Garnier *et al.* using DFT [20,23] inform the KMC simulations. Section II introduces the KMC algorithm used to compute Onsager matrices. Section III describes in detail the three derivative approaches for computing Onsager matrix derivatives with respect to strain, and the behavior of the statistical error for each approach. In Sec. IV, we use the computed statistical errors and true errors to quantitatively compare the performance of the three approaches for uncorrelated single vacancy diffusion in fcc Ni and for correlated vacancy-mediated Si diffusion in Ni. Finally, in Sec. V, we consider the computational efficiency in general.

II. KMC CALCULATION OF ONSAGER MATRICES

Kinetic Monte Carlo simulations evolve a system in time using stochastic trajectories [22]. The systems we consider evolve along each trajectory by a vacancy hopping from one site to the possible nearest neighboring sites. For state i , the hopping rate v_k^i for transition k is expressed from harmonic

*zeboli1@illinois.edu

†dtrinkle@illinois.edu

transition state theory [24],

$$v_k^i = v_0^i \exp(-E_k^i/k_B T), \quad (1)$$

where v_0^i is the attempt frequency, k_B is Boltzmann's constant, T is the temperature, and E_k^i is the corresponding migration energy. For each state in the trajectory, we calculate hopping rates and select an event based on a pseudorandom number u from a uniform distribution. The index q of the event selected satisfies [25]

$$\sum_{k=1}^{q-1} v_k^i < u v_{\text{tot}}^i \leq \sum_{k=1}^q v_k^i, \quad (2)$$

where $v_{\text{tot}}^i = \sum_{k=1}^{N_{\text{NN}}} v_k^i$ is the sum over all transition rates from state i , and N_{NN} is the number of nearest neighbors. The escape time is drawn from an exponential distribution, and the average value of the sum of all escape times over the trajectory is the sum of average escape times Δt_i from each state in the trajectory,

$$\Delta t_i = 1/v_{\text{tot}}^i. \quad (3)$$

From KMC simulations, we can extract the evolution time $t_j = \sum_{i=1}^{N_{\text{step}}} \Delta t_i$ for the j th trajectory, where N_{step} is the number of steps per trajectory. We also measure the total particle displacement $r_{\alpha,j}^A$ for species A along direction α ($\alpha = x, y, z$) during time t_j .

We compute the values and relative statistical errors of Onsager matrices from KMC simulations. The Onsager matrix L^{AB} connects the flux \vec{J}^A of species A to the gradient of the chemical potential μ^B of species B [14],

$$\vec{J}^A = - \sum_B L^{AB} \vec{\nabla} \mu^B. \quad (4)$$

The mean squared displacements of the moving species determine the components of Onsager matrices [26],

$$L_{\alpha\beta}^{AB} = \frac{c}{N_{\text{traj}}} \sum_{j=1}^{N_{\text{traj}}} \frac{r_{\alpha,j}^A r_{\beta,j}^B}{2t_j}, \quad (5)$$

where c is a trajectory-independent constant $c = \frac{1}{\Omega k_B T}$ for simulation cell volume Ω , and N_{traj} is the number of KMC trajectories. In the special case of single vacancy diffusion in bulk system, the diffusion properties of the system are fully characterized by the transport coefficients $L_{\alpha\beta}^{VV}$, which are proportional to the vacancy diffusivities $D_{\alpha\beta}$ in the dilute limit,

$$D_{\alpha\beta} = \frac{1}{c} L_{\alpha\beta}^{VV}. \quad (6)$$

Therefore, we will use variable $D_{\alpha\beta}$ for single vacancy diffusion in bulk Ni, and the more general notation $L_{\alpha\beta}^{AB}$ for vacancy-mediated diffusion of Si in Ni(Si) alloys. The relative statistical error of $L_{\alpha\beta}^{AB}$ is

$$\sigma(L_{\alpha\beta}^{AB}) = \frac{\sqrt{\text{var}(L_{\alpha\beta}^{AB})}}{L_{\alpha\beta}^{AB}}, \quad (7)$$

where $\text{var}(L_{\alpha\beta}^{AB})$ is the variance of $L_{\alpha\beta}^{AB}$ over different KMC trajectories.

III. DERIVATIVE APPROACHES AND STATISTICAL ERRORS

We apply three different approaches to calculate derivatives of the Onsager matrices with respect to strain: the finite difference (FD) method, the correlated finite difference (CFD) method, and the perturbation theory (PT) approach. The FD method is a direct approximation to compute Onsager matrix derivatives but it has the largest statistical errors. The CFD method is an improvement of the FD method that reduces the statistical errors by using correlated sampling. Alternatively, we use perturbation theory to develop an approach that works especially well for uncorrelated diffusion systems. We use two systems to examine the performance of the three methods: one is uncorrelated single vacancy diffusion in fcc Ni and the other is correlated vacancy-mediated diffusion of dilute Si in Ni. We apply a tetragonal strain $\epsilon_{\alpha\beta} = \epsilon \delta_{\alpha\beta} (2\delta_{\alpha x} - \delta_{\alpha y} - \delta_{\alpha z})$, which causes the lattice to expand along the x direction and contract along the y and z directions. We do not consider effects from shear strain or volumetric strain. Garnier *et al.* showed that for vacancy-mediated diffusion of Si in Ni, the influence of shear strain on the migration energies is small compared to the influence of tetragonal strain [23], and volumetric strain causes the migration energies of different atomic jumps to increase or decrease by the same amount which does not change the relative probabilities of trajectories.

A. Finite difference method

The finite difference (FD) method approximates the derivative of the Onsager matrix with respect to strain $L_{\alpha\beta}^{AB}$ using the central difference scheme as

$$L_{\alpha\beta}^{AB} \Big|_{\epsilon=0} = \frac{L_{\alpha\beta}^{AB}(h) - L_{\alpha\beta}^{AB}(-h)}{2h} + O(h^2), \quad (8)$$

where h is the finite difference step size. We obtain $L_{\alpha\beta}^{AB}(h)$ and $L_{\alpha\beta}^{AB}(-h)$ from independent KMC simulations on the positively strained and negatively strained diffusion systems, respectively. Approximating the derivative using Eq. (8) induces a truncation error with an asymptotic behavior of $O(h^2)$ [27,28]. Similar to $L_{\alpha\beta}^{AB}$, we compute the relative statistical error of $L_{\alpha\beta}^{AB}$ as

$$\begin{aligned} \sigma^{\text{FD}}(L_{\alpha\beta}^{AB}) &= \frac{\sqrt{\text{var}[L_{\alpha\beta}^{AB}(h)] + \text{var}[L_{\alpha\beta}^{AB}(-h)]}}{2h L_{\alpha\beta}^{AB}} \\ &\approx \frac{\sqrt{\text{var}[L_{\alpha\beta}^{AB}(0)]}}{\sqrt{2} h L_{\alpha\beta}^{AB}}, \end{aligned} \quad (9)$$

which is inversely proportional to the step size h .

Moreover, we expect $\sigma^{\text{FD}}(L_{\alpha\beta}^{AB})$ to be independent of the number of steps because the Onsager matrix variance $\text{var}(L_{\alpha\beta}^{AB})$ is independent of N_{step} . For the special case of single vacancy diffusion, the initial configurations of all the vacancy hops are identical so the average waiting time Δt_i defined in Eq. (3) is constant along the trajectories, i.e., $\Delta t_i = \Delta t$. The variance of

the vacancy diffusivity is

$$\begin{aligned} \text{var}(D_{\alpha\beta}) &= \frac{1}{N_{\text{traj}}(N_{\text{traj}} - 1)} \sum_{j=1}^{N_{\text{traj}}} \text{var}\left(\frac{r_{\alpha,j}^V r_{\beta,j}^V}{2t_j}\right) \\ &= \frac{\text{var}(r_{\alpha,j}^V) \text{var}(r_{\beta,j}^V)}{(N_{\text{traj}} - 1) N_{\text{step}}^2 \Delta t}. \end{aligned} \quad (10)$$

In the last equality, the vacancy displacements $r_{\alpha,j}^V$ and $r_{\beta,j}^V$ are sums of N_{step} uncorrelated jump vectors. Therefore, their variances $\text{var}(r_{\alpha,j}^V)$ and $\text{var}(r_{\beta,j}^V)$ are proportional to N_{step} , which cancels the N_{step}^2 term in the denominator. For the more

general vacancy-mediated solute diffusion, the analytically derived statistical error behavior is an approximation if the solute concentration is in the dilute limit.

B. Correlated finite difference method

The correlated finite difference (CFD) method introduces an artificial correlation between the KMC trajectories for the positively and negatively strained diffusion systems to reduce the statistical error [29,30]. The relative statistical error of CFD is

$$\sigma^{\text{CFD}}(L_{\alpha\beta}^{\prime AB}) = \frac{\sqrt{\text{var}[L_{\alpha\beta}^{\prime AB}(h)] + \text{var}[L_{\alpha\beta}^{\prime AB}(-h)] - 2\text{cov}[L_{\alpha\beta}^{\prime AB}(h), L_{\alpha\beta}^{\prime AB}(-h)]}}{2h L_{\alpha\beta}^{\prime AB}}, \quad (11)$$

where $\text{cov}[L_{\alpha\beta}^{\prime AB}(h), L_{\alpha\beta}^{\prime AB}(-h)]$ is the covariance between $L_{\alpha\beta}^{\prime AB}(h)$ and $L_{\alpha\beta}^{\prime AB}(-h)$. The covariance must be positive for the CFD method to have smaller statistical errors than the FD method. We ensure that the two simulations are correlated by using the same random number sequence to generate the trajectories. Since there is no difference between the two sets of trajectories as h goes to zero, the covariance $\text{cov}[L_{\alpha\beta}^{\prime AB}(h), L_{\alpha\beta}^{\prime AB}(-h)]$ approaches $\text{var}(L_{\alpha\beta}^{\prime AB}) > 0$ in this limit. Therefore, we expect $\text{cov}[L_{\alpha\beta}^{\prime AB}(h), L_{\alpha\beta}^{\prime AB}(-h)]$ to be positive for small h .

The covariance $\text{cov}[L_{\alpha\beta}^{\prime AB}(h), L_{\alpha\beta}^{\prime AB}(-h)]$ quantifies the difference between statistical errors $\sigma^{\text{FD}}(L_{\alpha\beta}^{\prime AB})$ and $\sigma^{\text{CFD}}(L_{\alpha\beta}^{\prime AB})$ and decreases linearly with small finite difference step size h . For simplicity, we still confine our discussion to single vacancy diffusion in which all the initial configurations of vacancy hops are identical. Therefore, if the positively strained system and the negatively strained system follow identical trajectories, the covariance yields

$$\begin{aligned} \text{cov}^*[D_{\alpha\beta}(h), D_{\alpha\beta}(-h)] &= \frac{\sum_{j=1}^{N_{\text{traj}}} \left[\frac{r_{\alpha,j}^{V*} r_{\beta,j}^{V*}}{2t_j^*} \Big|_{\epsilon=h} - D_{\alpha\beta}(h) \right] \left[\frac{r_{\alpha,j}^{V*} r_{\beta,j}^{V*}}{2t_j^*} \Big|_{\epsilon=-h} - D_{\alpha\beta}(-h) \right]}{N_{\text{traj}}(N_{\text{traj}} - 1)} \\ &= \left[1 - \left(\frac{\epsilon_{\alpha\alpha}}{\epsilon} \right)^2 h^2 \right] \left[1 - \left(\frac{\epsilon_{\beta\beta}}{\epsilon} \right)^2 h^2 \right] \frac{\Delta t^2(0)}{\Delta t(h) \Delta t(-h)} \text{var}[D_{\alpha\beta}(0)], \end{aligned} \quad (12)$$

where $*$ denotes that the quantity is computed by assuming that the two strained systems follow identical trajectories. The factors $[1 - (\frac{\epsilon_{\alpha\alpha}}{\epsilon})^2 h^2]$ and $[1 - (\frac{\epsilon_{\beta\beta}}{\epsilon})^2 h^2]$ and $\frac{\Delta t^2(0)}{\Delta t_j(h) \Delta t_j(-h)}$ come from the effects of the strain-induced lattice deformation and changes in the average waiting time, respectively. However, the trajectories of two strained systems cannot be exactly the same due to the strain difference. We assume that at a given step i , the vacancy in the positively and negatively strained systems has a probability p_i to choose different jumps and probability $1 - p_i$ to choose the same jump. The probability p_i quantifies the discrepancy between the rate tables of the two differently strained systems, which is constant during the simulation for the single vacancy diffusion system, i.e., $p_i(h) = p(h)$. We expand p to first order in h ,

$$p(h) = p(0) + \frac{\partial p}{\partial h} \Big|_{h=0} h + O(h^2). \quad (13)$$

A zero strain difference yields the same rate tables for the two systems so $p(0) = 0$. As h increases from zero, the two rate tables diverge, suggesting that $\frac{\partial p_i}{\partial h} \Big|_{h=0} > 0$. For the positively strained system, a fraction $1 - p_i$ of a trajectory is exactly the same as that of the negatively strained system, which contributes to the covariance $\text{cov}[D_{\alpha\beta}(h), D_{\alpha\beta}(-h)]$. The covariance $\text{cov}^*[D_{\alpha\beta}(h), D_{\alpha\beta}(-h)]$ changes by a factor of

$[1 - p(h)]$, such that

$$\begin{aligned} \text{cov}[D_{\alpha\beta}(h), D_{\alpha\beta}(-h)] &= [1 - p(h)] \text{cov}^*[D_{\alpha\beta}(h), D_{\alpha\beta}(-h)] \\ &= \left(1 - \frac{\partial p}{\partial h} \Big|_{h=0} h \right) \text{var}(D_{\alpha\beta}) + O(h^2), \end{aligned} \quad (14)$$

which indicates that the covariance decreases with h . Moreover, by comparing Eq. (14) with Eq. (11), we conclude that σ^{CFD} is proportional to $1/\sqrt{h}$ for small h . The statistical error of the CFD method σ^{CFD} is independent of N_{step} because there is no N_{step} dependence in Eq. (14).

C. Perturbation theory method

An alternative approach for computing the derivatives is based on the perturbation theory, which treats the tetragonal strain ϵ as a perturbation on the unstrained system. As ϵ is small, the vacancy in the perturbed system follows similar trajectories to the unperturbed system. We can compute Onsager matrices of the strained diffusion system by reweighing the trajectories based on relative probabilities from the unstrained system. The unnormalized probability that the vacancy in the strained system follows the j th unstrained trajectory is $\prod_{i=1}^{N_{\text{step}}} \gamma_i(\epsilon)$, where $\gamma_i(\epsilon) = \frac{v_q^i(\epsilon)}{v_{\text{tot}}^i(\epsilon)}$ is the probability that the vacancy takes the q th jump among N_{NN} possible choices at

the i th step of the j th trajectory, and $q = q(i, j)$ is the index of the jump that is selected at the given step for the unstrained system. Following the importance sampling [31–33], we use the probability ratios between the strained and unstrained systems to estimate the probability distribution for the strained trajectories and compute the ensemble average as

$$L_{\alpha\beta}^{AB}(\epsilon) = \frac{c}{\sum_{j=1}^{N_{\text{traj}}} P_j(\epsilon)} \sum_{j=1}^{N_{\text{traj}}} P_j(\epsilon) \frac{r_{\alpha,j}^A(\epsilon) r_{\beta,j}^B(\epsilon)}{2t_j(\epsilon)}, \quad (15)$$

where the reweighting factor is

$$P_j(\epsilon) = \prod_{i=1}^{N_{\text{step}}} \frac{\gamma_i(\epsilon)}{\gamma_i(0)}. \quad (16)$$

To obtain the strain derivative $L_{\alpha\beta}^{\prime AB}$ from Eq. (15), we expand all of the terms on the right-hand side to first order in ϵ . The reweighting factor $P_j(\epsilon)$ deviates from one as a result of the variation of the jump frequencies due to the migration energy changes, $E_k^i(\epsilon) = E_k^i(0) + \epsilon \frac{\partial E_k^i}{\partial \epsilon} + O(\epsilon^2)$,

$$P_j(\epsilon) = 1 + \frac{\epsilon}{k_B T} \sum_i \sum_{k=1}^{N_{\text{NN}}} \frac{v_k^i}{v_{\text{tot}}^i} \left(\frac{\partial E_k^i}{\partial \epsilon} - \frac{\partial E_q^i}{\partial \epsilon} \right) + O(\epsilon^2). \quad (17)$$

The species displacement $r_{\alpha,j}^A(\epsilon)$, a sum of strain-modified jump vectors, is

$$r_{\alpha,j}^A(\epsilon) = r_{\alpha,j}^A(0)(1 + \epsilon_{\alpha\alpha}). \quad (18)$$

The total evolution time $t_j(\epsilon)$ of each trajectory is an accumulation of waiting times $\Delta t_i(\epsilon)$, which follow

$$\Delta t_i(\epsilon) = \frac{1}{v_{\text{tot}}^i(\epsilon)} = \Delta t_i(0) + \epsilon \Delta t_i^2(0) \sum_{k=1}^{N_{\text{NN}}} \frac{v_k^i}{k_B T} \frac{\partial E_k^i}{\partial \epsilon} + O(\epsilon^2). \quad (19)$$

We compute the reweighted ensemble average by substituting Eqs. (17)–(19) into Eq. (15), and extract the derivative $L_{\alpha\beta}^{\prime AB}$ from the first order terms as

$$L_{\alpha\beta}^{\prime AB} \Big|_{\epsilon=0} = \frac{c}{N_{\text{traj}}} \sum_{j=1}^{N_{\text{traj}}} (\Gamma_{\alpha\beta,j} + R_{\alpha\beta,j} + \tau_{\alpha\beta,j}), \quad (20)$$

where

$$\begin{aligned} \Gamma_{\alpha\beta,j} &= \frac{1}{k_B T} \sum_i \sum_{k=1}^{N_{\text{NN}}} \frac{v_k^i}{v_{\text{tot}}^i} \left(\frac{\partial E_k^i}{\partial \epsilon} - \frac{\partial E_q^i}{\partial \epsilon} \right) \\ &\times \left[\frac{r_{\alpha,j}^A(0) r_{\beta,j}^B(0)}{2t_j(0)} - L_{\alpha\beta}^{AB}(0) \right] \end{aligned} \quad (21)$$

comes from the reweighting process,

$$R_{\alpha\beta,j} = \left(\frac{\epsilon_{\alpha\alpha}}{\epsilon} + \frac{\epsilon_{\beta\beta}}{\epsilon} \right) \frac{r_{\alpha,j}^A(0) r_{\beta,j}^B(0)}{2t_j(0)} \quad (22)$$

is the contribution due to the tetragonal strain-induced lattice deformation, and

$$\tau_{\alpha\beta,j} = \left(\frac{1}{t_j} \sum_{i=1}^{N_{\text{step}}} \Delta t_i^2 \sum_{k=1}^{N_{\text{NN}}} \frac{v_k^i}{k_B T} \frac{\partial E_k^i}{\partial \epsilon} \right) \frac{r_{\alpha,j}^A(0) r_{\beta,j}^B(0)}{2t_j(0)} \quad (23)$$

is due to the change in the average waiting time for each vacancy hop. We compute the relative statistical error as

$$\sigma^{\text{PT}}(L_{\alpha\beta}^{\prime AB}) = \frac{c}{L_{\alpha\beta}^{\prime AB}} \sqrt{\frac{\text{var}(\Gamma_{\alpha\beta,j} + R_{\alpha\beta,j} + \tau_{\alpha\beta,j})}{N_{\text{traj}} - 1}}. \quad (24)$$

Unlike the FD and CFD methods, the statistical error of the PT approach increases proportionally to the square root of number of steps. According to Eq. (24), the behavior of σ^{PT} is determined by the behavior of $\text{var}(\Gamma_{\alpha\beta,j} + R_{\alpha\beta,j} + \tau_{\alpha\beta,j})$, which is

$$\begin{aligned} \text{var}(\Gamma_{\alpha\beta,j} + R_{\alpha\beta,j} + \tau_{\alpha\beta,j}) &= \text{var}(\Gamma_{\alpha\beta,j}) + \text{var}(R_{\alpha\beta,j}) \\ &+ \text{var}(\tau_{\alpha\beta,j}) + 2\text{cov}(R_{\alpha\beta,j}, \Gamma_{\alpha\beta,j}) \\ &+ 2\text{cov}(\tau_{\alpha\beta,j}, \Gamma_{\alpha\beta,j}) + 2\text{cov}(R_{\alpha\beta,j}, \tau_{\alpha\beta,j}), \end{aligned} \quad (25)$$

where $\Gamma_{\alpha\beta,j}$, $R_{\alpha\beta,j}$, and $\tau_{\alpha\beta,j}$ are terms defined in Eqs. (21), (22), and (23) characterizing the contributions from the reweighting process, lattice deformation, and average waiting time changes, respectively. For the case of single vacancy diffusion, $R_{\alpha\beta,j}$ and $\tau_{\alpha\beta,j}$ equal the term $(r_{\alpha,j}^V)(r_{\beta,j}^V)/2t_j$ multiplied by constants. Therefore, according to Eq. (10), their variances $\text{var}(R_{\alpha\beta,j})$ and $\text{var}(\tau_{\alpha\beta,j})$ as well as their covariance $\text{cov}(R_{\alpha\beta,j}, \tau_{\alpha\beta,j})$ are independent of N_{step} . However, $\Gamma_{\alpha\beta,j}$ is a sum of N_{step} terms that are identically distributed and independent of each other, so its variance $\text{var}(\Gamma_{\alpha\beta,j})$ as well as the covariance $\text{cov}(R_{\alpha\beta,j}, \Gamma_{\alpha\beta,j})$ and $\text{cov}(\tau_{\alpha\beta,j}, \Gamma_{\alpha\beta,j})$ are proportional to N_{step} . The net effect is that the variance $\text{var}(\Gamma_{\alpha\beta,j} + R_{\alpha\beta,j} + \tau_{\alpha\beta,j})$ changes linearly with the number of steps or, equivalently, $\sigma^{\text{PT}} \propto \sqrt{N_{\text{step}}}$, for $N_{\text{step}} \gg 1$.

IV. COMPUTATIONAL RESULTS

A. Single vacancy diffusion in fcc Ni

We first compare the performance of the three approaches outlined above for single vacancy diffusion in Ni. We introduce one vacancy into a $6 \times 6 \times 6$ fcc Ni supercell with periodic boundary conditions imposed in all three directions. The vacancy diffusion in the unstrained system is isotropic and the random walk is uncorrelated. Introducing tetragonal strain $\epsilon_{\alpha\beta}$ breaks the cubic symmetry, but does not introduce correlation between successive hopping steps. We use KMC to generate trajectories of vacancy hops and compute the derivative of the vacancy diffusivity component D_{xx} with respect to strain ϵ using the three different derivative approaches. For the special case of single vacancy diffusion, the analytical solution for D_{xx}' is [14]

$$D_{xx}^{\prime \text{AS}} \Big|_{\epsilon=0} = \frac{1}{2} \sum_{k=1}^{N_{\text{NN}}} \left(2 \frac{\epsilon_{xx}}{\epsilon} - \frac{1}{k_B T} \frac{\partial E_k}{\partial \epsilon} \right) l_{kx}^2 v_0 \exp\left(-\frac{E_k}{k_B T}\right), \quad (26)$$

which we use as a reference value to evaluate the relative true errors $\epsilon^M = \left| \frac{D^M - D^{\prime \text{AS}}}{D^M} \right|$ ($M = \text{FD, CFD, PT}$). The jump vectors \vec{l}_k , attempt frequency v_0 , migration energies E_k , and their derivatives $\frac{\partial E_k}{\partial \epsilon}$ are from the DFT calculation by Garnier *et al.* [20,23]. When $\epsilon = 0$, all of the migration energies are identical, i.e., $E_k = E$, but their derivatives with respect to

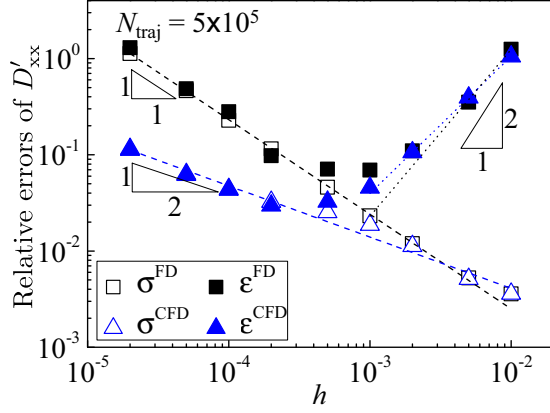


FIG. 1. Relative statistical errors σ and true errors ϵ of the strain derivative of diffusivity D'_{xx} as a function of the finite difference step size h for the FD and CFD methods. In all the plots, we use different shaped symbols to denote the errors from different methods: squares for FD and triangles for CFD (and diamonds for PT in the other figures). We use open symbols for the relative statistical errors σ and solid symbols for the relative true errors ϵ . We want the statistical errors to be a good estimate of the true errors so that the systematic errors are negligible. In this figure, the relative statistical errors decrease monotonically with increasing h . The statistical errors estimate the true errors well for small h . However, the good agreement between errors breaks down for h larger than 2×10^{-4} .

strain ϵ are not. We use the relative statistical errors σ^M calculated from Eqs. (9), (11), and (24), and the relative true errors ϵ^M to quantitatively compare the performance of the three methods. The relative true errors ϵ^M in Figs. 1–8 are root-mean-square (rms) true D' errors computed from multiple KMC runs with identical parameters. The true error contains the contributions from statistical fluctuations, as well as systematic errors which are difficult to assess quantitatively. However, the systematic errors are negligible when the statistical error is a good estimate of the true error.

Figure 1 shows that there is an optimal finite difference step size h for the FD and CFD methods that minimizes the statistical errors, and for which statistical errors are a good estimate of the true errors. The statistical errors of both approaches decrease monotonically with h . The relative statistical error of the FD method is inversely proportional to step size $\sigma^{\text{FD}} \propto 1/h$, which agrees with Eq. (9). For the CFD method, the statistical error σ^{CFD} stays below σ^{FD} and is inversely proportional to the square root of h , $\sigma^{\text{CFD}} \propto 1/\sqrt{h}$ for small h , which verifies the analytical behavior described in Eq. (14). When h increases, unlike the monotonically decreasing statistical errors, the truncation errors increase proportionally to h^2 as Eq. (8) shows. The truncation errors are non-negligible when h exceeds 2×10^{-4} , causing the true errors to deviate from the statistical errors. Based on our testing data points, we choose $h = 2 \times 10^{-4}$ so that statistical errors are minimal and remain a good estimate of the true errors.

Figures 2 and 3 show that the optimal number of KMC steps for uncorrelated diffusion systems is one. Figure 2 verifies that the relative statistical errors σ^{FD} and σ^{CFD} are independent of N_{step} as we expect, and $\sigma^{\text{PT}} \propto \sqrt{N_{\text{step}}}$ holds for all N_{step} values. Figure 3 shows that for fixed computational

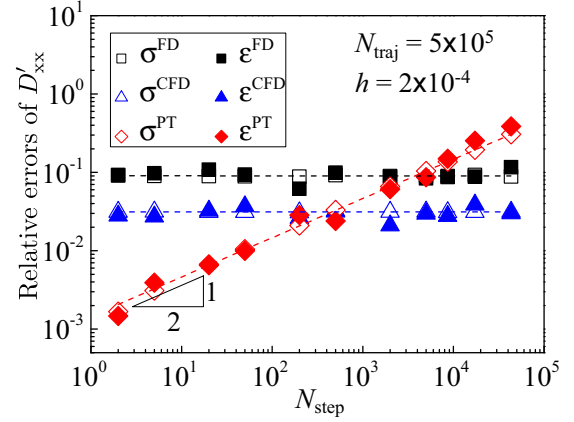


FIG. 2. Relative errors of D'_{xx} as a function of N_{step} for a fixed number of trajectories, $N_{\text{traj}} = 5 \times 10^5$. The relative statistical errors of the FD and CFD methods do not depend on N_{step} , while for the PT method, $\sigma^{\text{PT}} \propto \sqrt{N_{\text{step}}}$. The statistical errors estimate the true errors well for all values of N_{step} .

effort, defined as the total number of vacancy hops during one KMC run $N_{\text{tot}} = N_{\text{step}}N_{\text{traj}}$, all of the statistical errors increase monotonically with the number of steps. The FD and CFD methods have statistical errors that increase as $\sqrt{N_{\text{step}}}$, whereas the PT method statistical error increases faster as N_{step} . Using a larger number of steps means that a smaller number of trajectories can be applied, which leads to a direct increase in statistical errors. On the other hand, the figures also show that the statistical errors match the true errors across the entire range of N_{step} from 2 to 5×10^4 , which means reducing the number of steps in each trajectory does not introduce significant systematic errors. Therefore, the most efficient way to reduce the statistical errors of all three methods is setting $N_{\text{step}} = 1$, for which the KMC results extracted from the mean square displacements yield the analytical expression of Eq. (26).

Figure 4 shows that the PT approach has the best performance of the three methods for the uncorrelated diffusion

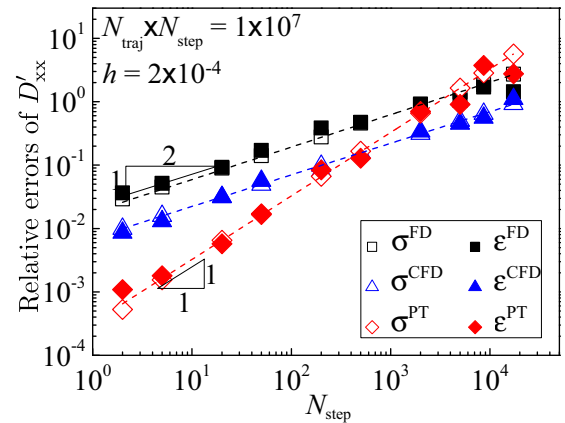


FIG. 3. Relative errors of D'_{xx} vs N_{step} for a fixed total computational effort, $N_{\text{tot}} = N_{\text{step}}N_{\text{traj}} = 10^7$. For the FD and CFD methods, σ^{FD} and $\sigma^{\text{CFD}} \propto \sqrt{N_{\text{step}}}$, whereas for the PT method, $\sigma^{\text{PT}} \propto N_{\text{step}}$. The statistical errors estimate the true errors well for all values of N_{step} .

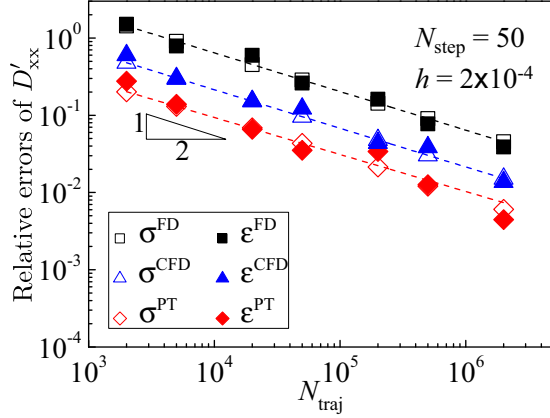


FIG. 4. Relative errors of D'_{xx} vs the number of trajectories N_{traj} . We choose h and N_{step} such that the statistical errors are a good estimate of the true errors. As N_{traj} increases, the statistical errors of all three methods decrease as $\sigma \propto 1/\sqrt{N_{traj}}$. The CFD method produces lower statistical errors than the FD method using correlated trajectories, and the PT method has the lowest statistical errors.

system. Even though the optimal number of steps is one, we use $N_{step} = 50$ and $h = 2 \times 10^{-4}$ to make an illustrative comparison between the three methods. All of the statistical errors follow $\sigma \propto 1/\sqrt{N_{traj}}$, and the PT approach has the lowest relative statistical and true errors. By reducing the number of steps, we can still decrease the errors of the PT method by up to a factor of $\sqrt{50} \approx 7$ for the same number of trajectories, but σ^{FD} and σ^{CFD} do not follow the same trend. Therefore, the PT approach is the best way to compute the diffusivity derivatives for the uncorrelated diffusion system.

B. Vacancy-mediated diffusion of Si in Ni

The second system that we use to test the three derivative approaches is vacancy-mediated Si diffusion in Ni, which is a correlated diffusion system. We introduce a vacancy and a substitutional Si atom into a $6 \times 6 \times 6$ fcc Ni supercell with periodic boundary conditions in all three directions. The vacancy hops are anisotropic because the jump frequencies depend on the relative position of the Si atom with respect to the vacancy. Moreover, successive vacancy hops are correlated due to the interaction between the vacancy and Si. We compute the derivative of the Onsager matrix component $L_{\alpha\beta}^{NiSi}$ with respect to strain ϵ and the corresponding statistical and true errors, σ and ϵ . We use the energy barriers and their derivatives with respect to strain for atomic jumps computed by Garnier *et al.* using DFT calculations [20,23]. The reference value of $L_{\alpha\beta}^{NiSi}$ used to compute the true errors is from the self-consistent mean field (SCMF) calculation by Garnier *et al.* [34].

Figure 5 shows that for vacancy-mediated diffusion of Si in Ni, the improved performance of using correlated sampling is not as effective as for single vacancy diffusion, whereas there still exists an optimal h that minimize the statistical errors while keeping the truncation errors negligible. Figures 5 and 1 differ since the statistical error of the CFD method for correlated diffusion (shown in Fig. 5) no longer strictly follows $\sigma^{CFD} \propto 1/\sqrt{h}$ for small h because the assumption we use to derive Eq. (14), i.e., that the initial configurations

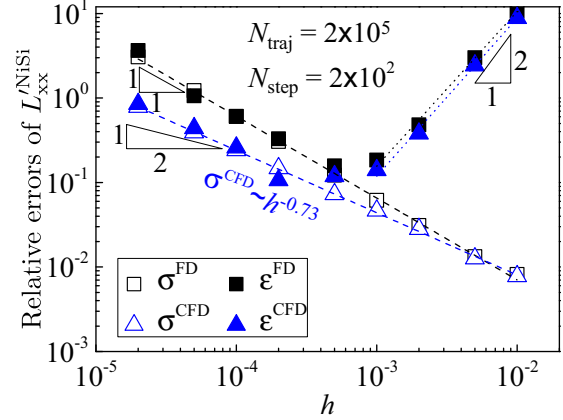


FIG. 5. Relative statistical and true errors of L'_{xx} as a function of finite difference step size h . Similarly to the single vacancy diffusion system, for both finite difference methods the statistical errors decrease monotonically with increasing h . The statistical errors are a good estimate of the true errors for small h , but the agreement breaks down for h larger than 2×10^{-4} .

of all vacancy hops are identical, no longer holds. We find that $\sigma^{CFD} \sim 1/h^{0.73}$, which lies between $1/\sqrt{h}$ and the upper bound $1/h$, suggesting that the correlation between the positively strained and negatively strained system is reduced for vacancy-mediated Si diffusion in Ni, but the covariance $\text{cov}[L_{\alpha\beta}^{AB}(h), L_{\alpha\beta}^{AB}(-h)]$ is still positive. However, similar to Fig. 1, the statistical errors for both FD and CFD methods decrease monotonically with h and closely match the true errors for $h < 2 \times 10^{-4}$. When h exceeds 2×10^{-4} , the true errors deviate from statistical errors due to the increasing truncation errors, which dominate the true errors for large h . The optimal value of h among our testing data points is 2×10^{-4} , which is when the truncation errors start to become comparable to the statistical errors.

Figures 6 and 7 show that among our testing data points, the optimal value of N_{step} that minimizes the statistical errors while having negligible systematic errors is 200. The statistical error

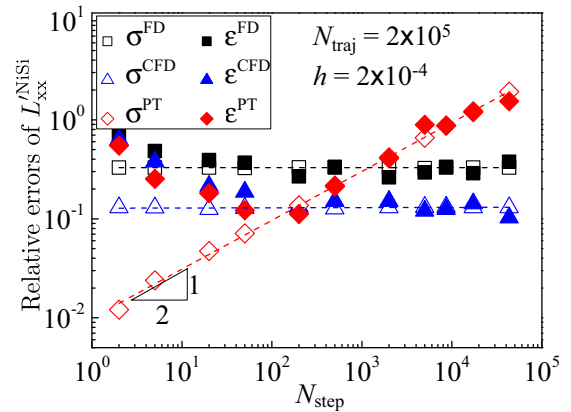


FIG. 6. Relative errors of L'_{xx} vs N_{step} for a fixed number of trajectories. The statistical errors behave similarly to those of the single vacancy diffusion system. However, the true errors behave differently: there is a threshold value of $N_{step} = 2 \times 10^2$ above which the statistical errors estimate the true errors well, while below this value the true errors become larger than the statistical errors.

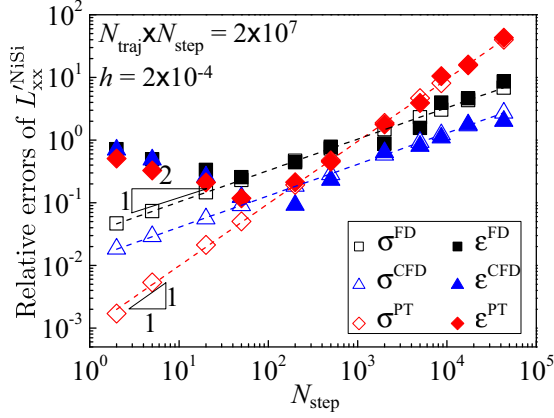


FIG. 7. Relative errors of L_{xx}^{NiSi} vs N_{step} for a fixed total computational effort $N_{\text{step}}N_{\text{traj}} = 2 \times 10^7$. The statistical errors behave similarly to those of the uncorrelated single vacancy diffusion system: σ^{FD} and $\sigma^{\text{CFD}} \propto \sqrt{N_{\text{step}}}$, while $\sigma^{\text{PT}} \propto N_{\text{step}}$. However, in this correlated case, there is a threshold value of $N_{\text{step}} = 2 \times 10^2$ above which the statistical errors are a good estimate of the true errors, while below this value the true errors become larger than the statistical errors.

curves in Fig. 6 follow the analytical behavior for uncorrelated diffusion that σ^{FD} and σ^{CFD} are independent of N_{step} , and σ^{PT} increases proportionally with $\sqrt{N_{\text{step}}}$. Therefore, similar to Fig. 3, for the same computational effort the statistical errors of all three methods can be reduced by decreasing the number of steps, as Fig. 7 shows. However, for correlated vacancy-mediated Si diffusion in Ni, there exists a minimum number of steps below which the statistical errors deviate from the true errors for all three methods due to a correlation-induced bias. Short trajectories, especially one-step trajectories, which work well for uncorrelated diffusion systems, produce large errors for the correlated diffusion system because they do not capture the correlation between successive vacancy hops. Theoretically, the correlation time of the system quantifies the lower bound of N_{step} that we can use to obtain good statistical results. Uncorrelated diffusion systems can be regarded as special cases with correlation time equal to zero. The true error curves in Figs. 6 and 7 verify the existence of the correlation-induced bias, which increases with decreasing number of steps and dominates the true error when N_{step} is small. We need to use long enough trajectories to make the correlation-induced bias negligible compared to the statistical errors. For all three methods, out of our testing data points, $N_{\text{step}} = 200$, is the minimum number of steps for which the statistical errors remain a good estimate of the true errors, i.e., for which the correlation-induced bias is negligible.

Figure 8 shows that the CFD method is the optimal approach to compute the strain derivative of L_{xx}^{NiSi} for vacancy-mediated Si diffusion in Ni. As is shown in Fig. 4, for single vacancy diffusion, the PT approach works better than the FD and CFD methods because we can employ short vacancy trajectories (as short as one step) without introducing significant systematic errors. For correlated diffusion, we need to use longer trajectories, i.e., larger N_{step} , to make sure that the correlation-induced bias is negligible. The statistical error of the PT approach is $\sigma^{\text{PT}} \propto \sqrt{N_{\text{step}}}$, which effectively shifts the σ^{PT} curve upwards

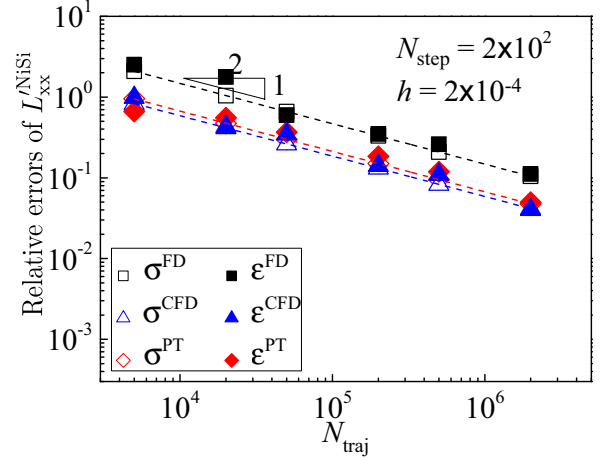


FIG. 8. Relative errors of L_{xx}^{NiSi} vs N_{traj} . We choose h and N_{step} such that the statistical errors estimate the true errors well. Similarly to the single vacancy diffusion system, as N_{traj} increases, the statistical errors of all three methods decay as $\sigma \propto \sqrt{N_{\text{traj}}}$. The CFD and PT methods give similar magnitudes of statistical errors, which are lower than those of the FD method.

relative to the σ^{FD} and σ^{CFD} curves, both of which do not depend on N_{step} for a fixed number of trajectories. We see from the figure that for vacancy-mediated Si diffusion in Ni, using the optimal value of 200 for the number of steps, the PT approach produces slightly larger statistical errors than the CFD method for the same number of trajectories. We expect that the CFD method will outperform the other two methods for systems with larger correlation times.

V. CONCLUSION

We compare the performance of the three derivative approaches, i.e., FD, CFD, and PT methods, for uncorrelated single vacancy diffusion in fcc Ni and for correlated vacancy-mediated Si diffusion in Ni. The FD method uses a central difference scheme to compute the derivatives by subtracting KMC results from systems with positive and negative strains. The CFD method is an improvement of the FD method, in which we apply the same random number sequence to create artificial correlation between the positively and negatively strained systems to reduce the statistical errors. We choose an appropriate finite difference step size h to minimize both the truncation errors and the statistical errors for the FD and CFD methods. The PT approach is an alternative way to compute derivatives, for which the statistical errors depend on the number of steps in each trajectory, $\sigma^{\text{PT}} \propto \sqrt{N_{\text{step}}}$, for fixed N_{traj} . The PT approach has the best performance of the three for uncorrelated diffusion systems, but performs worse for the correlated diffusion system in which a small number of steps causes a correlation-induced bias. For vacancy-mediated Si diffusion in Ni, the PT approach produces slightly larger statistical errors than those of the CFD method.

For the same computational effort, the PT approach requires less computational time than the other two methods. The FD and CFD methods require two KMC calculations for the positively strained and negatively strained systems separately, whereas the PT approach requires only one KMC

calculation. Therefore, obtaining derivatives using the PT approach requires about one-half the time of using the FD and CFD methods. The ratio of PT run time and the FD or CFD run time is not exactly half because PT requires three extra terms, i.e., $\Gamma_{\alpha\beta,j}$, $R_{\alpha\beta,j}$, and $\tau_{\alpha\beta,j}$ defined in Eqs. (21)–(23), but that can be faster than recomputing the table of rates at every hopping step.

The FD, CFD, and PT methods can compute other derivatives of physical quantities that can be extracted from KMC trajectories and can be applied to systems with stronger point defect interactions and more complicated crystal structures than Ni-Si alloys. We applied the derivative approaches to computing the derivatives of Onsager matrix components with respect to tetragonal strain for Ni with Si in the dilute limit. However, the methods are more general and can compute derivatives with respect to other changing variables such as temperature, external magnetic fields, or small radiation doses. The FD method requires a large number of KMC

trajectories to achieve acceptable statistical errors, and we find that the CFD and PT methods are more efficient since they require fewer trajectories to reach the same level of accuracy. For systems with stronger point defect interactions and more complicated crystal structures, successive diffusion steps are usually strongly correlated. In these cases, we expect the CFD method to outperform the PT approach because the longer KMC trajectories that we apply to eliminate the correlation-induced bias cause larger statistical errors for the PT approach, but do not affect the statistical errors of the CFD method.

ACKNOWLEDGMENTS

This research is partly supported by the US Department of Energy-BES Grant No. DE-FG02-05ER46217. The authors thank Thomas Schuler, Pinchao Zhang, and Michael Fellinger for helpful discussions.

-
- [1] A. J. Ardell and S. V. Prikhodko, Coarsening of γ' in Ni–Al alloys aged under uniaxial compression: II. Diffusion under stress and retardation of coarsening kinetics, *Acta Mater.* **51**, 5013 (2003).
 - [2] Dmitri A. Molodov, Tatiana Gorkaya, and Günter Gottstein, Migration of the $\Sigma 7$ tilt grain boundary in Al under an applied external stress, *Scr. Mater.* **65**, 990 (2011).
 - [3] Xuhang Tong, Hao Zhang, and Dongyang Li, Effects of misorientation and inclination on mechanical response of (110) tilt grain boundaries in α -Fe to external stresses, *Model. Simul. Mater. Sci. Eng.* **22**, 065016 (2014).
 - [4] S. M. Hafez Haghighat and R. Schäublin, Influence of the stress field due to pressurized nanometric He bubbles on the mobility of an edge dislocation in iron, *Philos. Mag.* **90**, 1075 (2010).
 - [5] M. R. Gilbert, S. Queyreau, and J. Marian, Stress and temperature dependence of screw dislocation mobility in α -Fe by molecular dynamics, *Phys. Rev. B* **84**, 174103 (2011).
 - [6] E. J. Savino, Point defect-dislocation interaction in a crystal under tension, *Philos. Mag.* **36**, 323 (1977).
 - [7] V. M. Chernov, D. A. Chulkin, and A. B. Sivak, Interaction of intrinsic point defects with dislocation stress fields in hcp zirconium crystal, *Crystallogr. Rep.* **55**, 83 (2010).
 - [8] A. B. Sivak, V. M. Chernov, N. A. Dubasova, and V. A. Romanov, Anisotropy migration of self-point defects in dislocation stress fields in BCC Fe and FCC Cu, *J. Nucl. Mater.* **367-370**, 316 (2007).
 - [9] Hui Yang, Minsheng Huang, and Zhenhuan Li, The influence of vacancies diffusion-induced dislocation climb on the creep and plasticity behaviors of nickel-based single crystal superalloy, *Comput. Mater. Sci.* **99**, 348 (2015).
 - [10] Yingxin Zhao, Qihong Fang, Youwen Liu, Pihua Wen, and Yong Liu, Creep behavior as dislocation climb over NiAl nanoprecipitates in ferritic alloy: The effects of interface stresses and temperature, *Int. J. Plastic.* **69**, 89 (2015).
 - [11] K. Sato, T. Yoshie, Y. Satoh, Q. Xu, E. Kuramoto, and M. Kiritani, Point Defect Production Under High Internal Stress Without Dislocations in Ni and Cu, *Radiat. Eff. Defects Solids* **157**, 171 (2002).
 - [12] M. P. Macht, A. Müller, V. Naundorf, and H. Wollenberger, Ion irradiation induced mass transport of Ni in Ni and Fe-20Cr-20Ni, *Nucl. Instrum. Methods Phys. Res. Sec. B* **16**, 148 (1986).
 - [13] A. Müller, V. Naundorf, and M. P. Macht, Point defect sinks in self-ion-irradiated nickel: A self-diffusion investigation, *J. Appl. Phys.* **64**, 3445 (1988).
 - [14] A. R. Allnatt and A. B. Lidiard, *Atomic Transport in Solids* (Cambridge University Press, Cambridge, 1993).
 - [15] F. C. Larché and J. W. Cahn, Overview No. 41 The interactions of composition and stress in crystalline solids, *Acta Metall.* **33**, 331 (1985).
 - [16] V. Nechaev and A. Viskovatykh, Effect of thermal stresses on the phase transition temperature in a ferroelectric-dielectric nanocomposite, *Phys. Solid State* **56**, 1992 (2014).
 - [17] F. Danoix, J. Lacaze, A. Gibert, D. Manginck, K. Hoummada, and E. Andrieu, Effect of external stress on the Fe–Cr phase separation in 15-5 PH and Fe–15Cr–5Ni alloys, *Ultramicroscopy* **132**, 193 (2013).
 - [18] C.-C. Lee, A. Fleurence, R. Friedlein, Y. Yamada-Takamura, and T. Ozaki, First-principles study on competing phases of silicene: Effect of substrate and strain, *Phys. Rev. B* **88**, 165404 (2013).
 - [19] P. H. Dederichs and K. Schroeder, Anisotropic diffusion in stress fields, *Phys. Rev. B* **17**, 2524 (1978).
 - [20] Thomas Garnier, Venkateswara R. Manga, Dallas R. Trinkle, Maylise Nastar, and Pascal Bellon, Stress-induced anisotropic diffusion in alloys: Complex Si solute flow near a dislocation core in Ni, *Phys. Rev. B* **88**, 134108 (2013).
 - [21] Wai-Lun Chan, Robert S. Averback, and Yinon Ashkenazy, Anisotropic diffusion of point defects in metals under a biaxial stress field simulation and theory, *J. Appl. Phys.* **104**, 023502 (2008).
 - [22] Corbett C. Battaile, The kinetic Monte Carlo method: Foundation, implementation, and application, *Comput. Methods Appl. Mech. Eng.* **197**, 3386 (2008).
 - [23] Thomas Garnier, Venkateswara R. Manga, Pascal Bellon, and Dallas R. Trinkle, Diffusion of Si impurities in Ni under stress: A first-principles study, *Phys. Rev. B* **90**, 024306 (2014).

- [24] George H. Vineyard, Frequency factors and isotope effects in solid state rate processes, *J. Phys. Chem. Solids* **3**, 121 (1957).
- [25] A. B. Bortz, M. H. Kalos, and J. L. Lebowitz, A new algorithm for Monte Carlo simulation of Ising spin systems, *J. Comput. Phys.* **17**, 10 (1975).
- [26] A. R. Allnatt, Einstein and linear response formulas for the phenomenological coefficients for isothermal matter transport in solids, *J. Phys. C* **15**, 5605 (1982).
- [27] A. R. Mitchell, Round-off errors in implicit finite difference methods, *Q. J. Mech. Appl. Math.* **9**, 111 (1956).
- [28] M. N. Spijker, On the structure of error estimates for finite-difference methods, *Numer. Math.* **18**, 73 (1971).
- [29] Tao He and Bingjing Su, On using correlated sampling to simulate small changes in system response by MCNP, *Ann. Nucl. Energy* **37**, 34 (2010).
- [30] Marcia O. Fenley, Michael Mascagni, James McClain, Alexander R. J. Silalahi, and Nikolai A. Simonov, Using correlated Monte Carlo sampling for efficiently solving the linearized Poisson-Boltzmann equation over a broad range of salt concentration, *J. Chem. Theory Comput.* **6**, 300 (2010).
- [31] Charles E. Clark, Importance sampling in Monte Carlo analysis, *Oper. Res.* **9**, 603 (1961).
- [32] Peter W. Glynn and Donald L. Iglehart, Importance sampling for stochastic simulations, *Mgmt. Sci.* **35**, 1367 (1989).
- [33] J.-C. Chen, D. Lu, J. S. Sadowsky, and K. Yao, On importance sampling in digital communications. I. Fundamentals, *IEEE J. Sel. Areas Commun.* **11**, 289 (1993).
- [34] Thomas Garnier, Zebo Li, Maylise Nastar, Pascal Bellon, and Dallas R. Trinkle, Calculation of strain effects on vacancy-mediated diffusion of impurities in fcc structures: General approach and application to $\text{Ni}_{1-x}\text{Si}_x$, *Phys. Rev. B* **90**, 184301 (2014).